Automated Interpretation of Myocardial SPECT Perfusion Images Using Artificial Neural Networks

Dan Lindahl, John Palmer, Mattias Ohlsson, Carsten Peterson, Anders Lundin and Lars Edenbrandt
Departments of Clinical Physiology, Radiation Physics, Theoretical Physics, and Radiology, Lund University, Lund, Sweden

The purpose of this study was to develop a computer-based method for automatic detection and localization of coronary artery disease (CAD) in myocardial bull's-eye scintigrams. **Methods:** A population of 135 patients who had undergone both myocardial ^{99m}Tc-sestamibi rest–stress scintigraphy and coronary angiography within 3 mo was studied. Different image data reduction methods, including pixel averaging and two-dimensional Fourier transform, were applied to the bull's-eye scintigrams. After a quantitative and qualitative evaluation of these methods, 30 Fourier components were chosen as inputs to multilayer perceptron artificial neural networks. The networks were trained to detect CAD in two vascular territories, using coronary angiography as gold standard. A "leave one out" procedure was used for training and evaluation. The performance of the networks was compared to those of two human experts. **Results:** One of the human experts detected CAD in one of two vascular territories, with a sensitivity of 54.4% at a specificity of 70.5%. The sensitivity of the networks was significantly higher at that level of specificity (77.2%, $p = 0.0022$). The other expert had a sensitivity of 63.2% at a specificity of 61.5%. The networks had a sensitivity of 77.2% ($p = 0.038$) at this specificity level as well. The differences in sensitivity between human experts and networks for the other vascular territory were all less than 6% and were not statistically significant. **Conclusion:** Artificial neural networks can detect CAD in myocardial bull's-eye scintigrams with such a high accuracy that the application of neural networks as clinical decision support tools appears to have significant potential.

Key Words: diagnosis; computer-assisted; artificial intelligence; neural networks; ischemic heart disease

J Nucl Med 1997; 38:1870–1875

Computer-aided interpretation of diagnostic images has gained much interest in the fields of radiology, nuclear medicine and magnetic resonance imaging (*1,2*). Computer technology can be used to support nonexperts with a preliminary interpretation in those situations in which experts are not present. Interpretation of diagnostic images is a pattern-recognition task, the result of which generally cannot be encapsulated in a set of criteria. Consequently, conventional rule-based expert systems have achieved only limited success in this area. Artificial neural networks represent a computer-based decision method that has proved to be of special value in pattern-recognition tasks (*3,4*). It is, therefore, of interest to evaluate the feasibility of using artificial neural networks for interpretation of diagnostic images. However, the large data content in diagnostic images causes problems in training the neural networks.

Artificial neural networks learn by example. The number of examples needed for network training depends on the size of the network. A large network that is fed with many input variables needs many examples to be trained properly. Images, especially in radiology but also in nuclear medicine and magnetic resonance imaging, contain large numbers of pixels. A commonly used image matrix in a scintigram is 256 × 256, i.e., 65,536 pixels. If all these pixel values were fed to a neural network, thousands of examples would be needed. The number of images available for training is typically on the order of 100. A substantial data reduction must, therefore, be performed, without loss of relevant information, before network training.

The purpose of this study was to develop a computer-based method to classify myocardial perfusion bull's-eye images. Different methods to reduce the data volume of the images were studied. Thereafter, artificial neural networks were trained to detect coronary artery disease (CAD). The performance of the networks was compared to those of two human experts, using coronary angiography as gold standard.

MATERIALS AND METHODS

Patient Population

All patients at Lund University Hospital, who, during the period from November 1992 to October 1994, had undergone both rest–stress myocardial perfusion scintigraphy and coronary angiography within 3 mo, were studied retrospectively. The total study population consisted of 166 patients, but 31 of these patients were excluded because they had undergone angioplasty or coronary artery bypass surgery or had signs of progressive CAD between the scintigraphy and angiography. The eligible study population, therefore, consisted of 135 patients, 94 men and 41 women (mean age, 56.7 yr; range, 21–77 yr). A contrast left ventriculogram was performed in 106 patients. The ejection fraction was normal in 65 patients, slightly to moderately reduced in 28 patients and severely reduced in 13 patients.

Coronary Angiography

Coronary angiography was used as gold standard. The patients were examined using the standard Judkins technique. Angiograms were performed and interpreted by experienced cardiac radiologists. Each coronary artery was examined in four to six projections, of which at least two were orthogonal. Significant CAD was defined as 75% or more lumen area reduction in a major coronary artery. The severity of a coronary stenosis was determined by visual assessment. The total myocardial perfusion bed was divided into two vascular territories. One assigned territory was the vascular bed of the left anterior descendent artery (LAD); the other territory was the vascular bed of the left circumflex artery (LCX) and the right coronary artery (RCA). Each territory was studied separately, regarding the presence or absence of CAD. In 41 patients, CAD was found in both the LAD and the RCA/LCX territories, and in 46 patients, CAD was found in one territory only (15 LAD and 31 RCA/LCX). Coronary angiography did not reveal significant CAD in the remaining 48 patients.

Myocardial Scintigraphy

Rest and stress studies were performed in a 1-day ^{99m}Tc-sestamibi protocol, using 300 MBq at rest and, after a delay of about 3 hr, 900 MBq at stress. The time period between injection and imaging was 1–2 hr for the rest studies and 30 min to 1 hr for the stress studies. Of the 135 patients studied, 131 underwent

Received Oct. 18, 1996; revision accepted Mar. 11, 1997.
For correspondence or reprints contact: Lars Edenbrandt, Department of Clinical Physiology, University Hospital, S-221 85 Lund, Sweden.

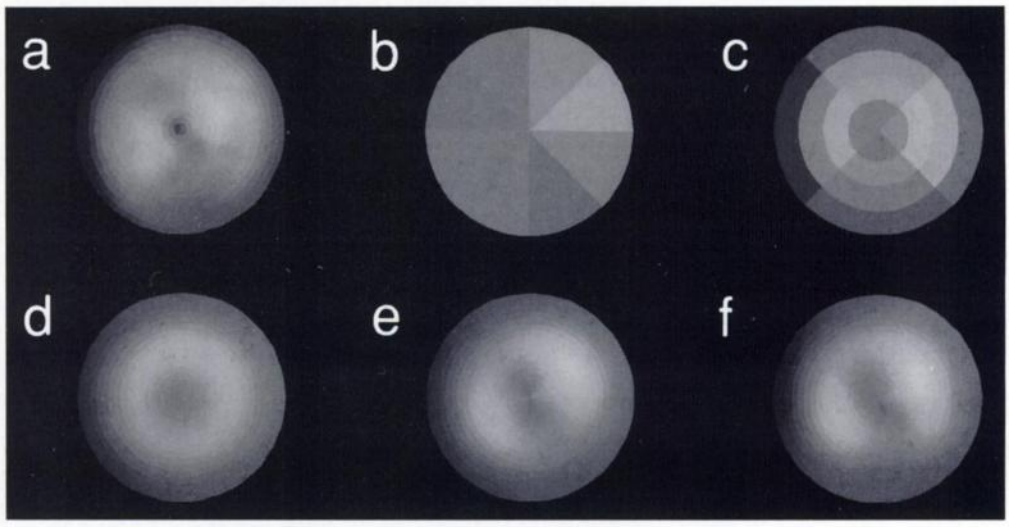

FIGURE 1. Comparison between original bull's-eye image (a) and the corresponding images reconstructed with different data reduction methods: coarsened images obtained by pixel averaging in 8 and 16 sectors (b and c, respectively) and images reconstructed from 18, 30 and 72 Fourier components (d–f, respectively).

exercise on a bicycle ergometer, and 4 were injected with dipyridamole (0.56 mg/kg). Exercise was symptom-limited (anginal pain, severe dyspnea or severe fatigue), unless malignant arrhythmia or exercise hypotension occurred (>10 mm Hg drop between exercise stages). Workload was increased in a stepwise manner, with 10 W/min. Exercise was continued for 1 min after injection.

The scintigraphy data were acquired in continuous SPECT over 180° over 20 min, with a 51 × 37 cm gamma camera, using a low-energy, high-resolution collimator (FWHM 9.7 mm at 15 cm) and a zoom factor of 1.5 (pixel size, 5.33 mm). Data were binned to 45 projection angles in a 64 × 64 matrix. Reconstruction was undertaken with standard techniques, using a two-dimensional Butterworth prereconstruction filter (*5*):

$$f(\omega) = 1/(1 + (\omega/\omega_c)^m),$$

with $m = 6$ and $\omega_c = 0.25$ cycles per pixel, followed by a ramp reconstruction filter.

A short-axis slice set was generated for entry into a bull's-eye (*6*) program, in which careful three-dimensional alignment of the rest and stress images was performed on an interactive basis by experienced clinical operators. This procedure included translations along the left ventricle axis and small corrections to the initially selected direction of this axis. Rotations about the axis were not made. After slice selection and positioning, data were sampled for the myocardial maximum in 64 radial directions for each slice including the apex. The sampled data were then linearly interpolated to exactly 17 slices and organized in a matrix map of 17 slices × 64 angles. The rest matrix, corrected for decay of ^{99m}Tc during the interval from rest to stress, was subtracted from the stress matrix as background. The maps were then normalized as follows. The rest map was scaled such that the average value of the region above 90% of its maximum was put to a fixed value,which was the same for all patients. The stress map was then scaled such that its average value, in the region above 90% of its maximum, was made equal to the average value of the rest map in a geometrically identical region. This normalization makes the rest and stress data equal in a region that is likely to be least ischemic and makes the absolute normalization dependent on the rest data only. The polar representation of these data was only used for visual classification; the neural networks worked exclusively on Cartesian data.

Image Data Reduction

To shrink the dimensionality of the artificial neural network input space, different image data preprocessing methods were evaluated. In Figure 1, an original rest image is presented in polar form together with five images reproduced using different data reduction methods. The original 17 × 64 image matrix was coarsened to 1 × 8 and 4 × 4 pixels, respectively, as shown in Figure 1, b and c. The resulting numbers of variables for rest–stress studies were 16 and 32, respectively. Figure 1, d–f, shows reconstructed rest images using a two-dimensional Fourier transform technique with inverse transformations of 18, 30 and 72 components for the rest–stress studies, respectively.

The following technique for extracting Fourier components from the rest and stress images was used. Each of the two 17 × 64 images was expanded by mirroring at about row 17 and then discarding the last row (i.e., the first row of the succeeding Fourier period), to produce 32 × 64 matrices. By this construction, only local data were, in effect, convoluted by the extraction of a few of all the available Fourier components, irrespective of slice location. The two 32 × 64 matrices were input as the real and imaginary parts of a complex 32 × 64 matrix in a fast Fourier transform (*7*). The spatial low-frequency components describing the rest and stress images are found near the origin in the spatial frequency plane, as mapped by the transformed complex matrix. Selections of up to 36 complex low-frequency components (72 real values) were made for further image analysis. Because the relative importance of axial and radial information is an a priori unknown, different sets of components were tried.

The number of components needed to reproduce the original rest and stress images in a satisfactory way was analyzed both quantitatively and qualitatively. The differences in pixel values of the original images and the corresponding values of the inverse-transformed data were studied using root mean-square (RMS) error calculations. A visual inspection of original and inverse-transformed images was also performed as in Figure 1. The best method, with consideration for both the amount of image reduction and differences between original and inverse-transformed images, was then used to calculate input variables to the artificial neural networks.

Neural Network

A multilayer perceptron neural network architecture (*8*) was used. The networks consisted of one input layer, one hidden layer and one output layer. The number of neurons in the input layer was equal to the number of input variables (30). The hidden layer contained three neurons and the output layer contained one neuron that encoded whether CAD was present or not. Three different sets of networks were studied, one that determines whether CAD was present or absent regardless of the location, one that detects CAD in the LAD territory and one that detects CAD in the RCA/LCX territory. The same type of network architecture and training parameters were used for the different networks.

During the training process, the connection weights between the neurons were adjusted using the back-propagation algorithm. The sigmoid activation function was used. The learning rate had a start value of 0.3. During the training, it was decreased between epochs. The momentum was set to 0.7. Updating occurred after every 20 patterns. The network weights were initiated with random numbers between −0.03 and 0.03. Training was set to stop at a training error of 0.36. All calculations were done using the JETNET 3.0 package (*9*).

The output values for test cases were in the range 0–1. A threshold in this interval was used above which all values were regarded as consistent with CAD. By varying this threshold, a receiver operating characteristic (ROC) curve was obtained.

"Leave One out" Procedure

To get a performance that was as reliable as possible, a "leave one out" validation procedure was used. One patient study was used as test case, whereas the remaining 134 cases were used for training. This procedure was repeated 135 times, such that each case in the dataset once was used as a test case. The test results of the 135 different networks were then concatenated, and the resulting list was used in the calculations of neural network performance.

Human Expert Classification

The performance of the networks was compared with those of two human experts. The bull's-eye images were presented to the experts in random order. Neither clinical data nor the results from angiography, neural networks or the classification of the other expert were available during the classification procedure. The experts had to rely on four bull's-eye images per patient study only: rest image, stress image, difference image and ratio image. They did not view short- or long-axis images. The experts classified each patient study and each vascular territory for the presence of CAD using a four-grade scale, as follows: "definitely not CAD," "probably not CAD," "probably CAD" and "definitely CAD."

Statistical Methods

Sensitivity and specificity for the assessment of CAD/no CAD by human experts were calculated and plotted together with the ROC curves for the networks. Areas under the ROC curves were calculated for the networks as a measure of performance. The four-grade scale used by the experts made it possible to calculate three sensitivity–specificity pairs for each expert. The comparisons between networks and experts were performed as follows. The threshold applied to the network outputs was chosen such that the specificity of the neural networks was the same as that of the expert. Thereafter, the corresponding sensitivity of the networks was compared to the sensitivity of the expert, and the significance of the difference in sensitivity was tested, paying attention to the fact that the same scintigrams were used; i.e., a McNemar type of statistic was used.

RESULTS

Image Data Reduction

The results of the quantitative comparison between the different image data reduction methods are presented in Figure 2. The RMS values of the Fourier-transformed and inverse-transformed images were lower than those of the images that were coarsened with pixel averaging compared at the same number of variables. An increase in the number of variables used to describe an image reduced the RMS error irrespective of the method used. In the images based on 9 complex Fourier components (18 values), small but clinically important perfusion defects are not reproduced satisfactorily. Most of the relevant information of the original images is contained in the images based on both 15 (30 values) and 36 complex components (72 values) (Fig. 1), but the RMS is not reduced in proportion to the increased number of components. For 72 values, the number of neurons in the network would exceed the number of training examples and, as a few preliminary runs indicated, the results did not improve. Therefore, 15 complex Fourier components were used as inputs to the artificial neural networks.

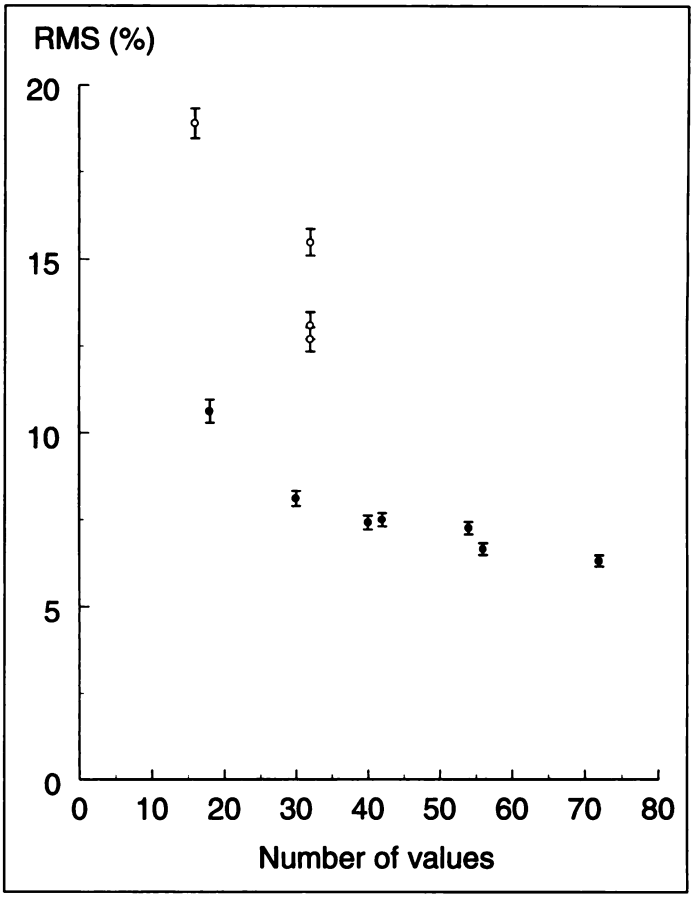

FIGURE 2. RMS values for reconstructed images using different image data reduction methods. ○, pixel averaging methods; ●, Fourier transform methods. The values shown are mean and s.e.m.

Image Classification

The ROC curve of the artificial neural networks detecting CAD in the LAD territory is presented in Figure 3, together with the specificity–sensitivity value pairs of the human experts. One of the experts had a sensitivity of 54.4% at a specificity of 70.5%. The sensitivity of the networks was 77.2% at that level of specificity. This difference in sensitivity of 22.8% was statistically significant ($p = 0.0022$). The other expert had a sensitivity of 63.2% at a specificity of 61.5%. At this specificity, the networks had a sensitivity of 77.2%, and this difference of 14.0% was also statistically significant ($p = 0.038$). No other differences in sensitivity between the experts and the networks were statistically significant.

The ROC curve of the networks detecting CAD in the RCA/LCX territory is presented in Figure 4. The area under this curve was 0.82, compared to the area under the LAD curve of 0.76. The networks determining CAD regardless of location had an area under the ROC curve of 0.80 (Fig. 5). The differences in sensitivity between experts and networks shown in the Figures 4 and 5 were all less than 6% and were not statistically significant.

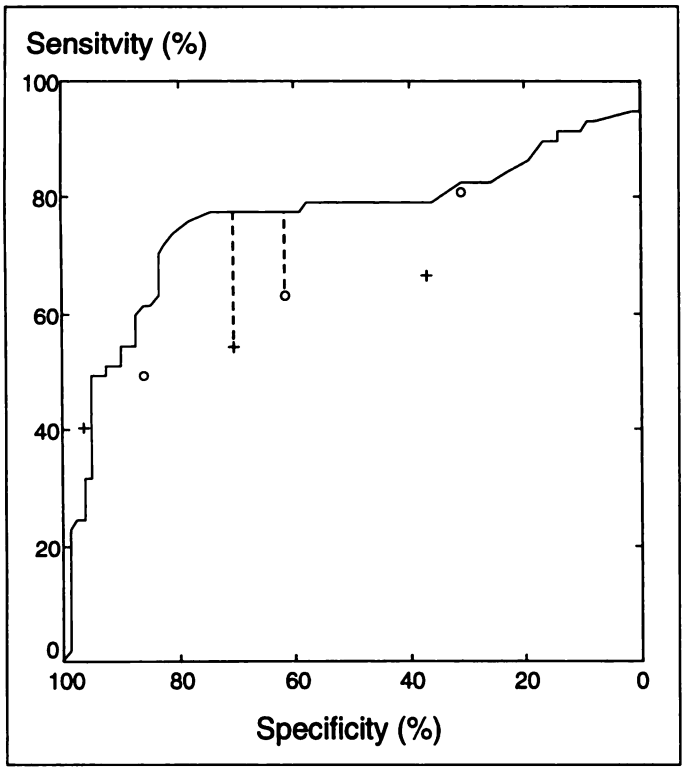

FIGURE 3. Classification performance for detecting CAD in LAD territory. The neural network performance is presented as an ROC curve, and experts' results are shown (○, expert 1; and +, expert 2). Statistically significant differences in sensitivity between networks and experts are indicated with vertical lines.

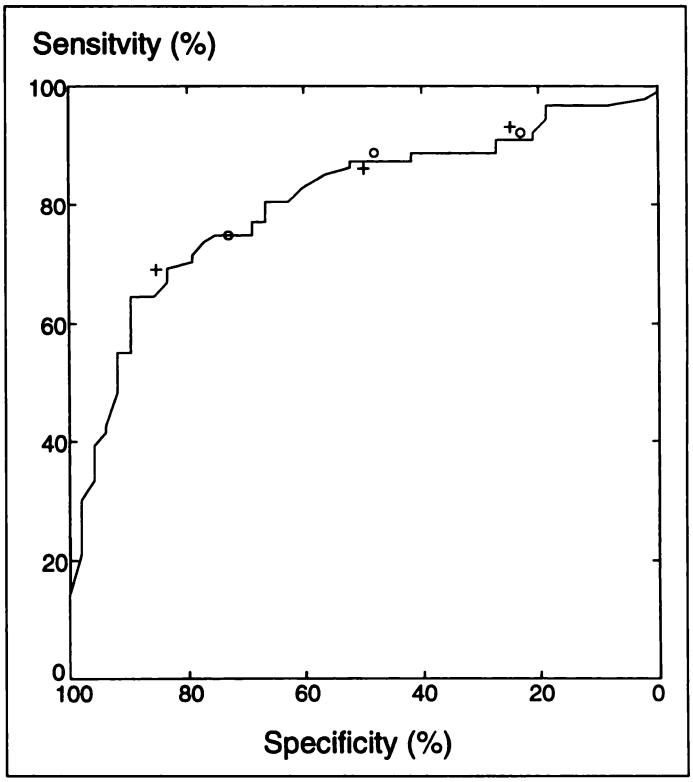

FIGURE 5. Classification performance for detecting CAD regardless of localization. Notation is the same as that in Figure 3.

DISCUSSION

We have demonstrated that artificial neural networks can be used to classify myocardial perfusion images regarding presence and locality of CAD. The performances of the networks were similar to or better than those of two human experts. These results indicate that neural networks could be used to assist clinicians in achieving a correct interpretation and, thereby, improve the diagnostic accuracy of medical imaging. An important ingredient in the computer-based method to classify bull's-eye images is the two-dimensional Fourier transform.

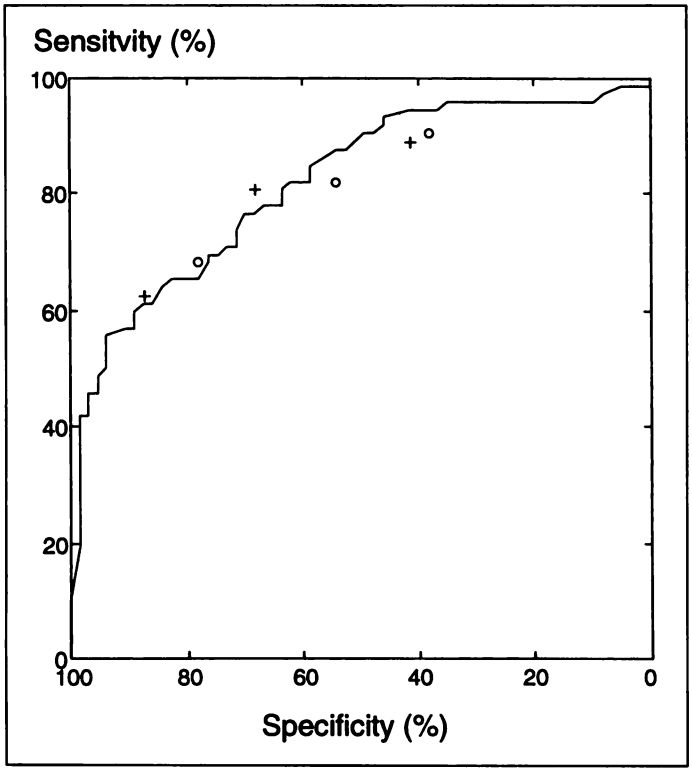

FIGURE 4. Classification performance for detecting CAD in the RCA/LCX territory. Notation is the same as that in Figure 3.

The networks detected CAD better in the RCA/LCX territory than they did in the LAD territory. The experts also performed better in the RCA/LCX territory. Neither the networks nor the experts could achieve a very high sensitivity, even at a low specificity in the LAD territory, as shown in Figure 3. These findings indicate that they cannot find scintigraphic abnormalities in the LAD territory in several cases with CAD according to coronary angiography. This could be due to an angiographic overestimation of lesion severity or functionally important coronary collaterals. However, the same disagreement between angiographic and scintigraphic findings were not found in the RCA/LCX territory.

Why Image Data Reduction?

When artificial neural networks are used, two things have to be considered regarding the input data. On one hand, it is an advantage to present as much information as possible to the network. On the other hand, a large number of inputs results in a network with many connection weights, and the network will require a large training database to generalize well. This is because the number of connection weights or fitted parameters depends strongly on the number of input neurons. The number of input neurons in a network is equal to the number of variables that are presented to the network. In general, the majority of weights in a neural network are connecting the input neurons and the hidden neurons.

Image data reduction with two-dimensional Fourier transform reduces the need for a large number of input neurons. The

30 variables used in this study contain information that is sufficient to reproduce the scintigrams in a satisfactory way, as shown in Figure 1. The method preserves more of the original image structure than do methods in which the matrix for each of the rest and stress images are coarsened to distinct predefined regions using pixel averaging. This superior performance is not surprising because the Fourier transform does not favor fixed spatial locations, as a predefined subdivision might do.

The Fourier transform is well-suited for the analysis of myocardial bull's-eye images. However, in applications for which the information content of the images lie both in the high- and low-spatial frequency domains, the method may need some additional modification or may be less suitable.

Another general approach that has been used is the "preclassification method." Human observers analyze the images and make classifications into several predefined classes, which are then used as input data (*10,11*). One problem with this method is the intra-and interobserver variability. The network could produce different output values for the same image if it is trained with different preclassifications. There is also a considerable risk that information missed by the observers is lost.

Requirements for the Training Material

The performance of an artificial neural network largely depends on the size and composition of the training database. Here, a database of 135 patients who had undergone both scintigraphy and coronary angiography was used. The training sets contained 134 patients, and the networks had 97 connection weights. The resulting ratio between the number of examples in the training set and the number of connection weights in the network was more than 1. Conversely, Fujita et al. (*12*) used 58 myocardial perfusion images to train networks that contained 26,500 connection weights. We find it remarkable that they designed a study around networks with so many weights and so few examples. Surprisingly, their networks correctly classified many of the cases in the test sets. One reason for this is probably the selection of cases in the database; 74 relatively typical cases from SPECT bull's-eye examinations were used. Cases for which the diagnoses obtained by angiography and scintigraphy differed were excluded.

Porenta et al. (*13*) trained neural networks containing more than 700 connection weights with less than 40 examples from myocardial scintigraphy with ^{201}Tl. Their networks performed significantly worse than did a human expert. We think this is due to the small number of examples relative to the number of connection weights.

The composition of the training set is as important as the number of examples. The examples must be representative of patient studies found in a clinical setting. Networks trained with a group of selected typical cases or cases with purely synthesized defects will not be useful in clinical practice. Because of the choice of clinical cases in our study, the results should give an accurate hint of the usefulness of neural networks in a clinical environment.

Expert Systems

Computer-aided decision support systems can be based on different methods from the field of artificial intelligence. The most widely used decision support systems, interpretation programs in computerized electrocardiographs, are generally based on conventional expert systems. Artificial neural networks have only recently been implemented in these programs. Expert systems have also been developed for interpretation of myocardial bull's-eye images (*14–16*), in which criteria for the detection of CAD were developed using separate normal limits in different predefined territories of the images. However, the visual interpretation of an image is generally not dependent on simple criteria; rather, to a great extent, it is a pattern-recognition task. Artificial neural networks have shown to be well-suited for this type of tasks. Networks have outperformed very complex expert systems, for example, electrocardiographic interpretation programs (*17*). Therefore, it was of interest to apply neural networks for the interpretation of bull's-eye images. One advantage with the neural network approach is the possibility of using Fourier transform components as inputs. These components constitute an unbiased description of the image, which is in contrast to the predefined parameters commonly used in expert systems.

The Choice of Gold Standard

Coronary angiography is considered to be the appropriate gold standard for the diagnosis of CAD. However, myocardial scintigraphy can provide additional information of clinical importance (*18*). For example, the extent and severity of ischemia, as reflected by the myocardial scintigraphy provide prognostic information in patients with known CAD.

We used coronary angiography as the gold standard because this provides an independent reference for the comparison of network and human experts. The results show that artificial neural networks can classify scintigrams in a search for CAD with angiography as the gold standard. We believe that networks could also classify scintigrams in a search for ischemia using human experts as the gold standard.

CONCLUSION

We found it possible to develop a computer-based method to classify myocardial perfusion bull's-eye images that performed as well as or better than a human expert. Artificial neural networks can detect CAD in myocardial bull's-eye scintigrams with such a high accuracy that the application of neural networks as clinical decision support tools appears to have significant potential.

ACKNOWLEDGMENTS

This study was supported by the Swedish Medical Research Council (Grant B95-14X-09893-04B), the Faculty of Natural Sciences at Lund University (Lund, Sweden), the Swedish National Board for Industrial and Technical Development and the Swedish Natural Science Research Council.

REFERENCES

1. Miller AS, Blott BH, Hames TK. Review of neural network applications in medical imaging and signal processing. *Med Biol Eng Comput* 1992;30:449–464.
2. Datz FL, Rosenberg C, Gabor FV, et al. The use of computer-assisted diagnosis in cardiac perfusion nuclear medicine studies: a review. *J Digit Imaging* 1993;6:67–80.
3. Cross SS, Harrison RF, Kennedy RL. Introduction to neural networks. *Lancet* 1995;346:1075–1079.
4. Baxt WG. Application of artificial neural networks to clinical medicine. *Lancet* 1995;346:1135–1138.
5. Gonzalez RC, Wintz P. *Digital image processing*, 2nd ed. Reading, MA: Addison Wesley; 1987:170–171.
6. Van Train KF, Garcia EV, Cooke D, Areeda J. Quantitative analysis of SPECT myocardial perfusion. In: DePuey EG, Berman DS, Garcia EV, eds. *Cardiac SPECT imaging*. New York: Raven Press; 1995:49–74.
7. Press WH, Teukolsky SA, Vetterling WT, Flammery BP. *Numerical recipes in C*, 2nd ed. Cambridge, UK: Cambridge University Press; 1995:521–525.
8. Rumelhart DE, McClelland JL, eds. *Parallel distributed processing*, Vols. 1 and 2. Cambridge, MA: MIT Press; 1986:318–362.
9. Peterson C, Rögnvaldsson T, Lönnblad L. JETNET 3.0: a versatile artificial neural network package. *Comput Phys Commun* 1994;81:185–220.
10. Scott JA, Palmer EL. Neural network analysis of ventilation-perfusion lung scans. *Radiology* 1993;186:661–664.
11. Tourassi GD, Floyd CE, Sostman HD, Coleman RE. Artificial neural network for diagnosis of acute pulmonary embolism: effect of case and observer selection. *Radiology* 1995;194:889–893.
12. Fujita H, Katafuchi T, Uehara T, Nishimura T. Application of artificial neural network to computer-aided diagnosis of coronary artery disease in myocardial SPECT bull's-eye images. *J Nucl Med* 1992;33:272–276.
13. Porenta G, Dorffner G, Kundrat S, Petta P, Duit-Schedlmayer J, Sochor H. Automated

interpretation of planar thallium-201-dipyridamole stress-redistribution scintigrams using artificial neural networks. *J Nucl Med* 1994;35:2041–2047.
14. Van Train KF, Areeda J, Garcia EV, et al. Quantitative same-day rest-stress technetium-99m-sestamibi SPECT: definition and validation of stress normal limits and criteria for abnormality. *J Nucl Med* 1993;34:1494–1502.
15. Van Train KF, Garcia EV, Maddahi J, et al. Multicenter trial validation for quantitative analysis of same-day rest-stress technetium-99m-sestamibi myocardial tomograms. *J Nucl Med* 1994;35:609–618.
16. Kahn JK, McGhie I, Akers MS, et al. Quantitative rotational tomography with 201-Tl and 99m-Tc 2-methoxy-isobutyl-isonitrile: a direct comparison in normal individuals and patients with coronary artery disease. *Circulation* 1989;79:1282–1293.
17. Hedén B, Edenbrandt L, Wesley K, Haisty JR, Pahlm O. Artificial neural networks for the electrocardiographic diagnosis of healed myocardial infarction. *Am J Cardiol* 1994;74:5–8.
18. Berman DS, Kiat H, Friedman JD, Diamond G. Clinical applications of exercise nuclear cardiology studies in the era of healthcare reform. *Am J Cardiol* 1995;75:3D–13D.

Quantification of Area at Risk in Acute Myocardial Infarction by Tomographic Imaging

Yuhji Furutani, Toshiaki Shiigi, Yasuma Nakamura, Hiroshi Nakamura, Masahiko Harada, Takeshi Yamamoto, Takatoshi Wakeyama, Masami Nakatsuka, Hiroshi Ogawa and Masunori Matsuzaki

Second Department of Internal Medicine, Yamaguchi University School of Medicine, Ube, and Division of Cardiology, Tokuyama Central Hospital, Tokuyama, Yamaguchi, Japan

The purpose of this study was twofold: to validate, in a phantom heart model, a simple threshold technique for the quantification of defect size using ^{123}I-15-(p-iodophenyl)-3-(R,S)-methyl pentadecanoic acid (BMIPP) imaging and to compare, in patients with acute myocardial infarction, defect size as shown by BMIPP imaging, with the extent of severe hypokinesis shown by left ventriculography. **Methods:** In a phantom study, defect size was calculated using a standard geometric formula. In a clinical study, BMIPP imaging was performed in 20 patients 10 ± 5 days after the onset of their infarction. Using the centerline method, the area at risk was defined by contrast ventriculography as the percentage of chords with wall motion >2 s.d. below normal. **Results:** In the phantom study, a threshold value of 60% yielded the best agreement between true and measured defect size. In the clinical study, the defect size shown by BMIPP imaging was greater in anterior than in inferior infarcts ($p < 0.001$) and correlated well with the risk area revealed by contrast ventriculography ($r = 0.80$, $p < 0.0001$) **Conclusion:** The above preliminary data, admittedly from a small group of patients, suggest that tomographic BMIPP imaging provides an accurate quantification of defect size by means of a simple threshold technique and, in the subacute phase, permits determination of the amount of myocardium at risk after acute myocardial infarction.

Key Words: BMIPP; area at risk; acute myocardial infarction

J Nucl Med 1997; 38:1875–1882

Fatty acids are the major fuel for the normal myocardium under normal aerobic conditions, and the use of ^{123}I-labeled fatty acids has been proposed for the investigation of the metabolism of the myocardium (*1*). Iodine-123-15-(p-iodophenyl)-3-(R,S)-methylpentadecanoic acid (BMIPP), an analog of pentadecanoic acid, may be useful for this purpose. A methyl group is introduced at the beta carbon to prolong its residence time in the myocardium, and a terminal para-phenyl group is added to stabilize the iodine label (*1*). The prolonged retention time allows for high-quality SPECT imaging, and, moreover, a more homogeneous distribution of the tracer in the left ventricular myocardium than that seen with ^{201}Tl is obtained in normal subjects (*2*). In patients with ischemic heart disease, the abnormality shown by BMIPP is generally more extensive than that seen with ^{201}Tl, probably because metabolic abnormality shows relatively more severe derangement than perfusion disturbance (*2–7*). The use of BMIPP in the subacute phase of infarction has been reported previously (*5,6*). Discordant segments with a relatively more reduced BMIPP uptake were observed more often in acute than in chronic myocardial infarction and more often in reperfused than in nonreperfused segments. A low uptake of BMIPP is thought to be due to a delayed recovery of fatty acid metabolism after reperfusion, and the mismatched areas could be used as a marker of salvaged myocardium or to delineate the area at risk (*5*).

Tomographic imaging with ^{99m}Tc-sestamibi has been used in the Nuclear Medicine Laboratory at the Mayo Clinic (Rochester, Minnesota) as a means of assessing the myocardium at risk, the infarct size and the efficacy of treatment in acute myocardial infarction (*8–10*). For the measurement of both the amount of myocardium at risk and the infarct size from such ^{99m}Tc-sestamibi tomographic images, a simple threshold method using a sum-of-cylinders technique to derive defect size from short-axis tomographic slices of the heart has been validated in a phantom model in that laboratory (*11*).

The purpose of this study was twofold. First, we wished, in a phantom model, to validate a simple threshold technique for the quantification of defect size from BMIPP SPECT images using short-axis tomographic slices. Second, we wished to determine whether, in the subacute phase in patients with acute myocardial infarction, use of such a technique would allow a noninvasive assessment of the area at risk. The latter we did by comparing the defect size shown by BMIPP SPECT imaging in the subacute phase with the extent of severe hypokinesis revealed by left ventriculography (LVG).

MATERIALS AND METHODS

Phantom Study

Left ventricular defect size was measured using ^{123}I in a version of the simple threshold technique validated for ^{99m}Tc in the Nuclear Medicine Laboratory at the Mayo Clinic (*11*). Tomographic acquisitions were performed using a static cardiac phantom. Because the myocardial-to-background activity ratio for BMIPP in normal subjects has been reported to be about 2 (*12*), the myocardial portion of the phantom was filled with a solution of ^{123}I that provided a myocardial-to-background activity ratio of this magnitude. Fifteen solid silicon insets, each of a size between 3.6% and 60% of myocardial volume, were introduced into the myocardial portion to simulate the desired defect. Figure 1 indicates the size of the myocardial defect and its anatomical location. Some of these infarct locations are unlikely to occur in clinical practice, but they were included so that the effects of diametrically opposed lesions on the estimation of defect size could be studied. A total of 16 SPECT acquisitions were performed, one for each of the 15

Received Aug. 26, 1996; revision accepted Feb. 3, 1997.
For correspondence or reprints contact: Yuhji Furutani, MD, Second Department of Internal Medicine, Yamaguchi University School of Medicine, 1144 Kogushi, Nishi-ku, Ube, Yamaguchi 755, Japan.